High Angular Resolution Studies of the Structure and Evolution of Protoplanetary Disks

by

Joshua A. Eisner

ISBN: 1-58112-280-2

DISSERTATION.COM

Boca Raton, Florida
USA • 2005

High Angular Resolution Studies of the Structure and Evolution of Protoplanetary Disks

Dissertation.com
Boca Raton, Florida
USA • 2005

ISBN: 1-58112-280-2

High angular resolution studies of the structure and evolution of protoplanetary disks

Thesis by
Joshua A. Eisner

In Partial Fulfillment of the Requirements
for the Degree of
Doctor of Philosophy

California Institute of Technology
Pasadena, California

2005
(Defended May 17, 2005)

Cover Illustration:
An artist's concept of a low-mass star surrounded by a rotating disk of dust and gas.
Credit NASA/JPL-Caltech/T. Pyle (SSC).

Acknowledgements

The work presented in this thesis has benefited greatly from my interactions with many people. First and foremost are my advisors, Lynne Hillenbrand and Anneila Sargent. While working with two advisors is somewhat unusual, I found it it be an incredibly rewarding experience. Lynne and Anneila are both great scientists and teachers, and I learned a lot from them about the science of star and planet formation, as well as the techniques by which to study these subjects. I also fed off of their enthusiasm, and was often spurred onward by their suggestions and ideas.

There are several other people I would like to thank for their roles in my intellectual and professional development. Shri Kulkarni, my first advisor at Caltech, taught me a great deal about how to think and write about science, and this knowledge continues to serve me well. Ben Lane also played an important role in this thesis, teaching me many of the details of near-infrared interferometry, and working many a night with me at PTI. Two of the chapters in this thesis are co-authored by John Carpenter and myself, testifying to the large role he has played in my research. It has been a pleasure working with John and having the opportunity to absorb some of his ideas and approach. I would also like to thank my other collaborators and mentors, all of whom have been great to interact with and learn from: Rachel Akeson, Stuartt Corder, Lincoln Greenhill, James Herrnstein, Karl Menten, Stanimir Metchev, James Moran, Russel White, and Sebastian Wolf.

I am grateful to the staff at the Palomar and Keck observatories, the PTI collaboration, and the Robotic P60 team for all of their help. Without them, the data presented in this thesis would not have been obtained, and I greatly appreciate their efforts. I am also grateful for the friendship and good humor of those with whom I have had the pleasure to observe. Kevin Rykoski in particular enriched my experience at Palomar. He taught me many subtleties of PTI, obtained some great data for me during his observing nights, and always kept his sense of humor, ensuring good spirits even on nights when everything else was going wrong.

The Caltech Astronomy department is a great place to learn about many different areas of astronomy, and to bounce ideas off of great astronomers. I am happy to have had the chance to interact with faculty, postdocs, and graduate students in the Robinson lounge and during informal office visits. Several conversations with Re'em Sari and Geoff Blake, among others, have helped me greatly to crystallize my understanding of issues related to this dissertation. I'm also indebted to my friends in the Caltech astronomy department (and the larger IPAC/JPL community), without whom maintaining my sanity during the more intense periods of my PhD career would have been substantially more difficult. So I whole-heartedly thank Josh, Kevin, Stan, Dave, Gordon, Dan, Don, Stefanie, and all the

others who I haven't mentioned.

I also thank my family for their contributions to this work. My parents supported and encouraged me throughout my life, and helped me find a path to a life of intellectual pursuits. And my wife, Kelly, has been with me through thick and thin. She put up with me for five years of observing runs, late nights, and low income. The real thanks will be that I will now be able to keep her in the way to which she has become accustomed.

Finally, I gratefully acknowledge the financial support provided by the Michelson Graduate Fellowship program, which aims to advance the development and application of high angular resolution astronomical instruments, including optical/near-IR interferometry. This dissertation was performed in part under contract with the Jet Propulsion Laboratory (JPL) funded by NASA through the Michelson Fellowship Program. JPL is managed for NASA by the California Institute of Technology.

Abstract

Young stars are surrounded by massive, rotating disks of dust and gas, which supply a reservoir of material that may be incorporated into planets or accreted onto the central star. In this dissertation, I use high angular resolution observations at a range of wavelengths to understand the structure, ubiquity, and evolutionary timescales of protoplanetary disks.

First, I describe a study of Class I protostars, objects believed to be at an evolutionary stage between collapsing spherical clouds and fully-assembled young stars surrounded by protoplanetary disks. I use a Monte Carlo radiative transfer code to model new 0.9 μm scattered light images, 1.3 mm continuum images, and broadband spectral energy distributions. This modeling shows that Class I sources are probably surrounded by massive protoplanetary disks embedded in massive infalling envelopes. For the best-fitting models of the circumstellar dust distributions, I determine several important properties, including envelope and disk masses, mass infall rates, and system inclinations, and I use these results to constrain the evolutionary stage of these objects.

Second, I discuss observations of the innermost regions of more evolved disks around T Tauri and Herbig Ae/Be stars, obtained with the Palomar Testbed and Keck Interferometers. I constrain the spatial and temperature structure of the circumstellar material at sub-AU radii, and demonstrate that lower-mass stars are surrounded by inclined disks with puffed-up inner edges 0.1-1 AU from the star. In contrast, the truncated inner disks around more massive stars may not puff-up, indicating that disk structure depends on stellar properties. I discuss the implications of these results for disk accretion, terrestrial planet formation and giant planet migration.

Finally, I put these detailed studies of disk structure into a broader context by constraining the mass distribution and evolutionary timescales of circumstellar disks. Using the Owens Valley Millimeter Array, I mapped the millimeter continuum emission toward > 300 low-mass stars in the NGC 2024 and Orion Nebula clusters. These observations demonstrate that the average disk mass in each cluster is comparable to the "minimum-mass protosolar nebula", and that there may be disk evolution on one million year timescales.

Contents

Acknowledgements **v**

Abstract **vii**

1 Introduction **1**
1.1 Star and Planet Formation: The Role of Disks . . . 2
1.1.1 Disk Formation . . . 2
1.1.2 Disk Evolution . . . 2
1.1.3 Disk Accretion . . . 4
1.1.4 Planet Formation . . . 5
1.2 Evidence for Disks around Young Stars . . . 6
1.3 Open Questions . . . 8
1.3.1 Planet Formation . . . 8
1.3.2 Disk Accretion . . . 9
1.3.3 Circumstellar Geometry . . . 10
1.3.4 Environmental Effects . . . 11
1.4 Outline of Thesis . . . 11

2 Observational Techniques and Instruments **13**
2.1 Motivation for Interferometry . . . 13
2.2 Theory of Interferometry . . . 14
2.3 Relation of Fringes to Source Properties . . . 19
2.3.1 Modeling Visibilities . . . 20
2.4 Astronomical Interferometers . . . 22
2.4.1 Palomar Testbed Interferometer . . . 22
2.4.2 Keck Interferometer . . . 25
2.4.3 Owens Valley Millimeter Array . . . 26
2.4.4 Signal-to-Noise Considerations . . . 27

3 Constraining the Evolutionary Stage of Class I Protostars: Multi-wavelength Observations and Modeling **29**
3.1 Introduction . . . 29
3.2 Observations . . . 31
3.2.1 The Sample . . . 31
3.2.2 OVRO Observations . . . 33

3.2.3 Keck/LRIS Observations at 0.9 μm wavelength . . . 33
3.2.4 Keck/LWS Observations . . . 35
3.2.5 SEDs . . . 35
3.3 Modeling . . . 35
3.3.1 Rotating, Infalling Envelope . . . 40
3.3.2 Flared Disk . . . 45
3.3.3 Envelope+Disk . . . 48
3.3.4 Disk+Extinction Model . . . 50
3.4 Results . . . 51
3.4.1 Results for Individual Sources . . . 52
3.4.1.1 IRAS 04016+2610 . . . 52
3.4.1.2 IRAS 04108+2803B . . . 56
3.4.1.3 IRAS 04239+2436 . . . 56
3.4.1.4 IRAS 04295+2251 . . . 59
3.4.1.5 IRAS 04381+2540 . . . 59
3.5 Discussion . . . 62
3.5.1 Large-Scale Geometry . . . 63
3.5.2 Disk and Envelope Masses . . . 64
3.5.3 Evolutionary Stage . . . 66
3.5.4 Further Constraints on the Horizon . . . 67
3.6 Conclusions . . . 68
3.7 Appendix: LRIS Images of Larger Sample . . . 70

4 Near-Infrared Interferometric Measurements of Herbig Ae/Be Stars 73
4.1 Introduction . . . 73
4.2 Observations and Calibration . . . 75
4.3 Results . . . 78
4.3.1 Visibility Corrections . . . 79
4.3.2 Photometry . . . 81
4.3.3 Models . . . 82
4.3.3.1 Gaussian Model . . . 82
4.3.3.2 Uniform Disk Model . . . 83
4.3.3.3 Accretion Disk Model . . . 83
4.3.3.4 Ring Model . . . 84
4.3.3.5 Two-Component Model . . . 85
4.3.4 Modeling of Individual Sources . . . 85
4.3.4.1 AB Aur . . . 91
4.3.4.2 VV Ser . . . 91
4.3.4.3 V1685 Cyg . . . 92
4.3.4.4 AS 442 . . . 92
4.3.4.5 MWC 1080 . . . 92
4.4 Discussion . . . 94
4.5 Summary . . . 97
4.6 Appendix: Distance Estimates . . . 97

5 Resolved Inner Disks around Herbig Ae/Be Stars 99
5.1 Introduction . . . 99
5.2 Observations and Calibration . . . 100
5.2.1 PALAO Observations . . . 104
5.3 Modeling . . . 105
5.3.1 Visibility Corrections . . . 105
5.3.1.1 Nearby Companions . . . 105
5.3.1.2 Stellar Emission . . . 105
5.3.1.3 Extended Emission . . . 106
5.3.2 Compact Circumstellar Emission . . . 107
5.3.2.1 Simple Geometrical Disk Models . . . 108
5.3.2.2 Geometrically Flat Accretion Disk Model . . . 110
5.3.2.3 Puffed-Up Inner Disk Model . . . 111
5.3.2.4 Binary Model . . . 113
5.4 Results and Analysis . . . 113
5.4.1 PTI Results . . . 113
5.4.1.1 AB Aur . . . 119
5.4.1.2 MWC 480 . . . 120
5.4.1.3 MWC 758 . . . 120
5.4.1.4 CQ Tau . . . 120
5.4.1.5 T Ori and MWC 120 . . . 122
5.4.1.6 MWC 297 . . . 122
5.4.1.7 VV Ser . . . 123
5.4.1.8 V1295 Aql . . . 123
5.4.1.9 V1685 Cyg . . . 125
5.4.1.10 AS 442 . . . 125
5.4.1.11 MWC 1080 . . . 126
5.4.2 Comparison with K and H-band IOTA Visibilities . . . 126
5.4.3 Binaries . . . 130
5.4.4 Spectral Energy Distributions . . . 130
5.5 Discussion . . . 136
5.5.1 Unresolved Sources . . . 136
5.5.2 Disk Inclinations . . . 136
5.5.3 Inner versus Outer Disk Structure . . . 137
5.5.4 Vertical Disk Structure . . . 138
5.6 Summary . . . 139

6 Observations of T Tauri Disks at Sub-AU Radii: Implications for Magnetospheric Accretion and Planet Formation 141
6.1 Introduction . . . 141
6.2 Observations and Data Reduction . . . 143
6.2.1 Sample . . . 143
6.2.2 2.2 μm Interferometry . . . 143
6.2.3 JHK Adaptive Optics Imaging . . . 145

6.2.4 $UBVRI$ Photometry . . . 145
6.2.5 High Resolution Optical Spectroscopy . . . 147
6.3 Analysis . . . 147
6.3.1 Stellar and Accretion Properties . . . 149
6.3.1.1 Stellar Properties . . . 149
6.3.1.2 Mass Accretion Rates . . . 150
6.3.1.3 Magnetospheric Radii . . . 152
6.3.1.4 Co-Rotation Radii . . . 153
6.3.2 Near-IR Stellar and Excess Fluxes . . . 153
6.3.3 Modeling Inner Disk Structure . . . 154
6.3.4 Large-Scale Disk Structure . . . 159
6.4 Results for Individual Sources . . . 159
6.4.1 AS 207A . . . 160
6.4.2 V2508 Oph . . . 161
6.4.3 AS 205A . . . 161
6.4.4 PX Vul . . . 162
6.5 Discussion . . . 163
6.5.1 Emerging Properties of Inner Disks around T Tauri Stars . . . 163
6.5.2 Dust Sublimation and Magnetospheric Truncation . . . 164
6.5.3 Implications for Planet Formation . . . 166
6.6 Conclusions . . . 167
6.7 Appendix: Spectroscopic Binary AS 205B . . . 168

7 Distribution of Circumstellar Disk Masses in the Young Cluster NGC 2024 171
7.1 Introduction . . . 172
7.2 The NGC 2024 Cluster . . . 173
7.3 Observations . . . 175
7.4 λ3mm Continuum Emission . . . 177
7.5 Circumstellar Masses . . . 183
7.6 Discussion . . . 184
7.7 Conclusions . . . 187

8 Distribution of Circumstellar Disk Masses in the Orion Nebula Cluster 189
8.1 Introduction . . . 189
8.2 Observations and Data Reduction . . . 192
8.3 Results . . . 193
8.4 Discussion . . . 198

9 Summary and Future Prospects 201
9.1 Class I Protostars: Circumstellar Evolution and Accretion . . . 201
9.2 Inner Disk Structure: Planet Formation and Disk Accretion . . . 202
9.3 Disk Masses: Disk Evolution and Giant Planet Formation . . . 203

Bibliography 204

List of Tables

3.1 Spectral energy distributions for our sample . . . 36
3.1 Spectral energy distributions for our sample . . . 37
3.1 Spectral energy distributions for our sample . . . 38
3.2 Best-fit Models . . . 53
3.3 Comparison of compact and large-scale millimeter emission . . . 54

4.1 Observed Sources . . . 76
4.2 Summary of Observations . . . 77
4.3 Properties of Calibrator Sources . . . 79
4.4 Results of Modeling for AB Aur . . . 91
4.5 Results of Modeling for VV Ser . . . 92
4.6 Results of Modeling for V1685 Cyg . . . 93
4.7 Results of Modeling for AS 442 . . . 93
4.8 Results of Modeling for MWC 1080 . . . 94
4.9 Comparison with Hillenbrand et al. (1992) Models . . . 95
4.10 Comparison with Dullemond et al. (2001) Models . . . 96

5.1 Observed Sources . . . 101
5.2 Summary of Observations . . . 102
5.2 Summary of Observations . . . 103
5.3 Properties of Calibrator Sources . . . 104
5.4 Uniform Disk Models . . . 114
5.5 Gaussian Models . . . 115
5.6 Ring Models . . . 115
5.7 Geometrically Flat Accretion Disk Models . . . 116
5.8 Flared Disk Models with Puffed-Up Inner Walls . . . 117
5.9 Binary Models . . . 118
5.10 Accretion Disk Models for PTI+IOTA Visibilities . . . 129
5.11 Disk Parameters from Near-IR Interferometry and SEDs . . . 134

6.1 Observed Properties of Sample . . . 144
6.2 Photometry of Observed Sources . . . 146
6.3 Binaries . . . 147
6.4 Inferred Stellar and Accretion Properties . . . 151
6.5 Disk Parameters from Near-IR Interferometry and SEDs . . . 156
6.6 Measured versus Predicted Inner Disk Sizes . . . 158

7.1 Sources detected in λ3mm continuum with OVRO 179

8.1 Sources detected in λ3 mm continuum with OVRO 196

List of Figures

1.1 Observational classification of the star formation process 3
1.2 Velocity-weighted CO image of the young star AB Aur 6
1.3 Disk-like distributions of gas and dust in Orion 6
1.4 Scattered light images of IRAS 04302+2247 and HH 30 7
1.5 Near-IR excess fraction as a function of stellar age 8

2.1 Diagram of the classic two-slit experiment 15
2.2 Illustration of the interference pattern observed for an off-axis source 16
2.3 Illustration of the interference pattern observed for a binary source 17
2.4 Interference pattern for polychromatic light 18
2.5 Visibilities for uniform disk models 20
2.6 Brightness distributions and visibilities for uniform disk models 21
2.7 Photograph of the Palomar Testbed Interferometer 23
2.8 Sky coverage of the three PTI baselines 24
2.9 Photograph of the Keck Interferometer 25
2.10 Photograph of the Owens Valley Millimeter Array 27

3.1 λ1.3 mm images of Class I sample 32
3.2 λ0.9 μm images of Class I sample 34
3.3 Dependence of envelope model on $\dot{M}$ 42
3.4 Dependence of envelope model on $R_{\rm c}$ 43
3.5 Dependence of envelope model on $R_{\rm out}$ 44
3.6 Dependence of envelope model on inclination 45
3.7 Dependence of disk model on $M_{\rm disk}$ 46
3.8 Dependence of disk model on h_0 47
3.9 Dependence of disk model on $R_{\rm out}$ 48
3.10 Dependence of disk model on inclination 49
3.11 Dependence of disk+envelope model on $M_{\rm disk}$ 50
3.12 Best-fit models for IRAS 04016+2610 55
3.13 Best-fit models for IRAS 04108+2803B 57
3.14 Best-fit models for IRAS 04239+2436 58
3.15 Best-fit models for IRAS 04295+2251 60
3.16 Best-fit models for IRAS 04381+2540 61
3.17 Radial profiles of λ1.3 mm emission of best-fit models for IRAS 04016+2610 . 65
3.18 λ0.9 μm scattered light images of larger sample 71

4.1 Best-fit inclined uniform disk models and uv sampling for AB Aur, VV Ser, V1685 Cyg, AS 442, and MWC 1080 80
4.2 V^2 data from PTI and IOTA, and best-fit models for AB Aur 86
4.3 V^2 data and models for AB Aur, as a function of hour angle 86
4.4 V^2 data from PTI and best-fit models for VV Ser 87
4.5 V^2 data and models for VV Ser, as a function of hour angle 87
4.6 V^2 data from PTI and best-fit models for V1685 Cyg 88
4.7 V^2 data and models for V1685 Cyg, as a function of hour angle 88
4.8 V^2 data from PTI and best-fit models for AS 442 89
4.9 V^2 data and models for AS 442, as a function of hour angle 89
4.10 V^2 data from PTI and IOTA, and best-fit models for MWC 1080 90
4.11 V^2 data and models for MWC 1080, as a function of hour angle 90

5.1 Best-fit uniform disk models and uv sampling for AB Aur, MWC 480, MWC 758, CQ Tau, T Ori, MWC 120, MWC 297, VV Ser, V1295 Aql, V1685 Cyg, AS 442, and MWC 1080 109
5.2 V^2 PTI data and best-fit models for AB Aur 119
5.3 V^2 PTI data and best-fit models for MWC 480 120
5.4 V^2 PTI data and best-fit models for MWC 758 121
5.5 V^2 PTI data and best-fit models for CQ Tau 121
5.6 V^2 PTI data and best-fit models for T Ori 122
5.7 V^2 PTI data and best-fit models for MWC 120 123
5.8 V^2 PTI data and best-fit models for VV Ser 124
5.9 V^2 PTI data and best-fit models for V1295 Aql 124
5.10 V^2 PTI data and best-fit models for V1685 Cyg 125
5.11 V^2 PTI data and best-fit models for AS 442 126
5.12 V^2 PTI data and best-fit models for MWC 1080 127
5.13 PTI and IOTA V^2 data, and best-fit models for AB Aur, T Ori, MWC 297, V1295 Aql, V1685 Cyg, and MWC 1080 128
5.14 Measured and predicted SEDs for geometrically flat accretion disks 131
5.15 Measured and predicted SEDs for flared, puffed-up disks 132
5.16 Inner disk size versus stellar luminosity for HAEBEs 135

6.1 Keck/HIRES spectra of T Tauri stars 148
6.2 Measured SEDs and V^2, and best-fit models for AS 207A 160
6.3 Measured SEDs and V^2, and best-fit models for V2508 Oph 161
6.4 Measured SEDs and V^2, and best-fit models for AS 205A 162
6.5 Measured SEDs and V^2, and best-fit models for PX Vul 163
6.6 Model images and predicted truncation radii for T Tauri sample 165
6.7 Keck/HIRES spectrum of double-lined spectroscopic binary AS 205B 168

7.1 Color-magnitude diagram for the stars in the NGC 2024 cluster 174
7.2 Pointing positions for the NGC 2024 OVRO mosaic 176
7.3 uv coverage and synthesized beam of OVRO observations 177
7.4 λ3mm continuum mosaic of NGC 2024 178

7.5 Spatially-filtered λ3mm continuum mosaic of NGC 2024 180
7.6 λ3mm flux distribution for low-mass near-IR cluster members 181
7.7 Average image of 3mm emission for low-mass cluster members 182

8.1 JHK mosaic of the Orion Nebula cluster 191
8.2 Pointing positions for the ONC OVRO mosaic 192
8.3 λ3 mm continuum mosaic of the ONC 194
8.4 Noise distribution in the ONC OVRO mosaic 195
8.5 3 mm flux distribution and average image for near-IR cluster members 197
8.6 Disk mass, as a function of cluster age 199

Chapter 1

Introduction

Some of the central questions in astronomy, and indeed human inquiry in general, revolve around the formation of our solar system. How did our sun form? How did planets form out of the primordial circumstellar disk? Is the formation process universal, or is it unique to our own system? The answers to these questions are an integral part of understanding our place in the Universe.

With the discovery of a planet orbiting a main-sequence star other than our own sun (Mayor & Queloz 1995), and the subsequent discovery of over 100 extra-solar planets including multiple-planet systems (e.g., Marcy & Butler 2000; Butler et al. 1999), it is clear that planets are not unique to our own solar system. However, these extra-solar planets have properties that differ substantially from planets in our solar system, suggesting that the conditions that gave rise to our own system may not be universal. Studying the initial conditions of star and planet formation is crucial to understanding how planetary systems are created.

Direct observations of young stars and planets are difficult because of the small angular sizes of these objects and the high brightness contrast between stars and planets, especially at optical wavelengths. While astronomical instruments are now on the horizon that will allow a direct view of young stars and planets in formation, with current telescopes we are still limited to indirect observations. We therefore focus on the study of primordial material associated with forming stars and planets, which is more easily observed with current instruments.

As originally suggested by Kant, and later Laplace, the fact that the planets in our solar system lie in a common orbital plane suggests that our system formed out of a flattened, rotating, disk-like structure. It is believed that protoplanetary disks provide the birthsites for planetary systems around other stars as well, and the fairly recent discovery of dust and gas-rich disks around young stars supports this notion. Because circumstellar disks are larger than either stars or planets, and usually brighter at longer wavelengths due to the reprocessing of stellar light by dense dusty material, disks can be studied with current astronomical instruments and techniques. However, the challenges to observing circumstellar disks around young stars remain severe because, at typical distances to regions of star formation ($\gtrsim$ 140 pc), the sizes of disks are beyond the angular resolution of most astronomical telescopes.

In this thesis, we describe high angular resolution observations of circumstellar disks that can resolve their spatial structure on scales relevant to both terrestrial and giant planet for-

mation. By studying the ubiquity, evolutionary timescales, and structure of protoplanetary disks around young stars, we place crucial constraints on the formation and evolution of planetary systems. These observations help to place our own solar system in context, and provide insight into our place in the Universe.

1.1 Star and Planet Formation: The Role of Disks

1.1.1 Disk Formation

In the canonical theories of star formation, a giant molecular cloud initially supported by thermal and magnetic pressure begins to collapse under the influence of gravity, aided by ambipolar diffusion (e.g., Shu et al. 1987, 1993). As collapse continues, the density in some regions of the cloud increases (thus decreasing the Jeans Mass), and these high-density regions may fragment into molecular cloud cores. These cores continue to collapse, and since they typically contain at least a small amount of angular momentum, if only because of differential Galactic rotation, material in the outer regions cannot fall directly onto the star, but instead creates a rotating disk (e.g., Ulrich 1976; Cassen & Moosman 1981; Terebey et al. 1984).

Simple geometrical arguments can be used to estimate the size of the disk (e.g., Ulrich 1976; Cassen & Moosman 1981): conservation of angular momentum dictates that for a collapsing cloud with specific angular momentum j and central mass M_*, the angular velocity at the edge of the disk, R_c, is

$$\Omega^2 = \frac{j^2}{R_c^4} = \frac{GM_*}{R_c^3}. \tag{1.1}$$

Assuming $M_* = 0.5$ M$_\odot$ and $j = 6 \times 10^{20}$ cm^2 s^{-1} (Goodman et al. 1993), we obtain $R_c \approx 300$ AU. Thus, we expect that young stars will be surrounded by sizable disks of dust and gas.

1.1.2 Disk Evolution

Disks represent a stage in the process of star and planet formation that is probably intermediate to spherical collapsing clouds and fully assembled main-sequence stars surrounded by planets. Although disk evolution is a continuous process, discrete evolutionary classes have been defined that provide a useful framework in which to describe different stages of disk life-cycles. Disk evolution is typically divided into four observationally-determined evolutionary classes, Classes 0, I, II, and III (Figure 1.1). This classification scheme was originally defined based on infrared spectral index and the ratio of sub-millimeter to bolometric luminosity (Lada & Wilking 1984; Lada 1987; Adams et al. 1987; André et al. 1993), and it has subsequently been shown to be consistent with other observational indicators, including mid-IR spectral index (Myers et al. 1987) and bolometric temperature (Myers & Ladd 1993).

This evolutionary sequence is illustrated in Figure 1.1, and described below. Class 0 objects are thought to be true protostars, surrounded by roughly spherical collapsing envelopes from which forming young stars are still accreting substantial fractions of their final mass. Because of the very high columns of cold dust in these envelopes, these objects emit most

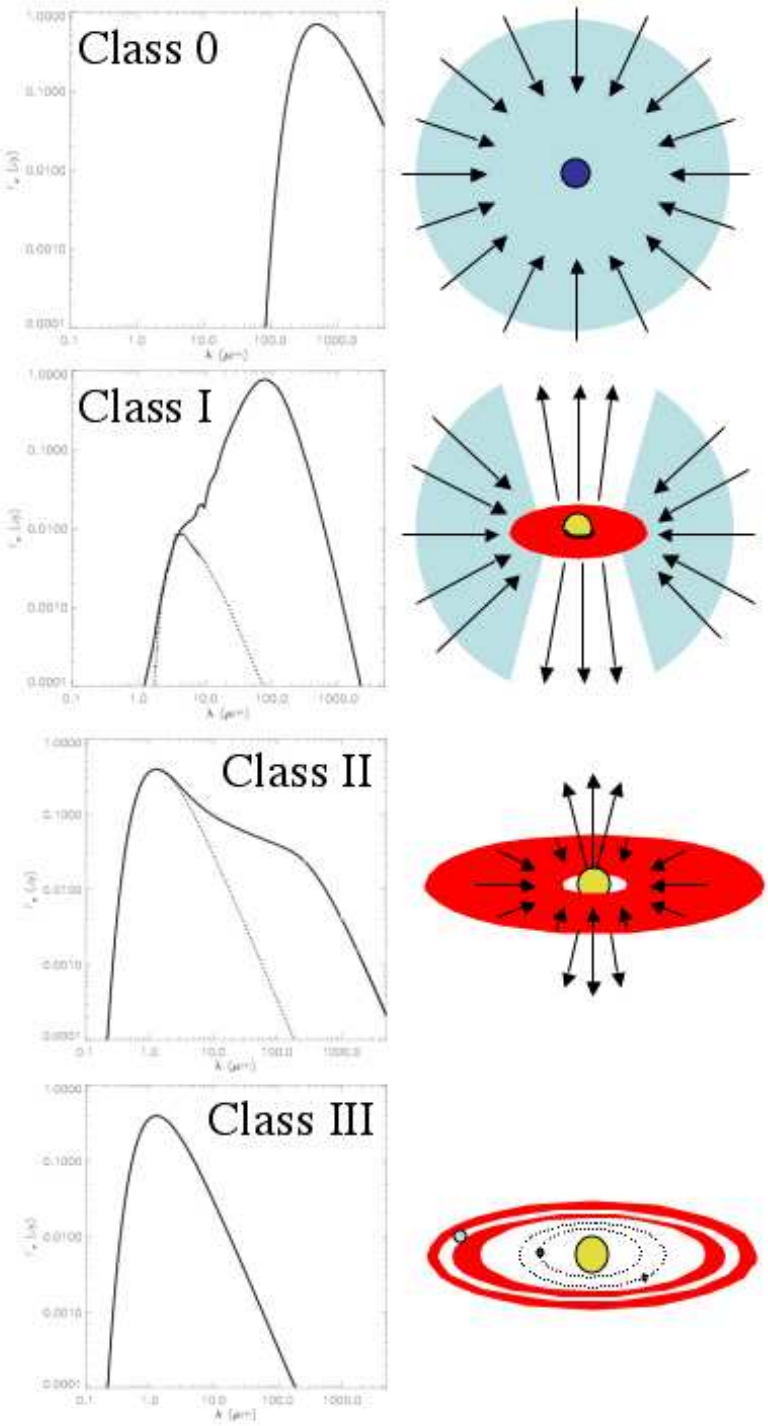

Figure 1.1 Observational classification of the star formation process. The left panels show the spectral energy distributions that typify members of the different evolutionary classes, and on the right we sketch the approximate geometry for each stage.

of their radiation at sub-millimeter wavelengths. Class I objects are still deeply embedded and have high mass accretion rates, but have begun to clear away material from the polar regions because of strong outflows. These sources are still not directly visible, and emit most of their radiation at far-IR wavelengths due to reprocessing of the stellar radiation by warm dust. Class II sources are optically-visible young stars, which have probably already assembled almost all of their final mass, but which still show excess emission at infrared and millimeter wavelengths indicative of optically-thick circumstellar disks. Finally, Class III sources appear to be pre-main-sequence stars that have already depleted most or all of the material in their circumstellar disks, and therefore show little or no infrared emission in excess of that expected from the stellar photosphere.

1.1.3 Disk Accretion

During the various phases of disk evolution, material in the disk accretes inward onto the central star, losing angular momentum in the process (e.g., Shakura & Sunyaev 1973; Lynden-Bell & Pringle 1974). Various mechanisms have been proposed for angular momentum transfer, and different processes may be operative at different stages of disk evolution. Hydromagnetic outflows are one possible way to remove angular momentum from disk material (e.g., Blandford & Payne 1982; Shu et al. 1994). Since energetic, collimated outflows may only exist in the early stages of disk evolution (with substantially weaker or no outflows for Class II and III objects), and magnetic outflows may only couple with the hot, ionized inner disk regions, outflows cannot provide a complete explanation for how angular momentum is transported in disks. Angular momentum may also be transported by gravitational instabilities (e.g., Papaloizou & Savonije 1991; Laughlin & Bodenheimer 1994). Since this process occurs only in massive disks, gravitational instability is probably most important for less evolved objects like Class I sources, where massive envelopes provide a large reservoir of material still building up the disk. For lower mass disks, or systems that have already undergone gravitational instability and thereby depleted much of their mass (e.g., Class II objects), angular momentum must be transported by viscous processes, and the most prominent theory of viscosity in circumstellar disks is the "magneto-rotational instability" (MRI; Balbus & Hawley 1991). However, MRI requires an ionized disk for magnetic coupling, and thus may not operate everywhere in disks (e.g., Gammie 1996).

Magnetic fields may also be important in regulating accretion from the innermost disk regions onto the central stars. The paradigm for accretion onto the central star (at least for low-mass stars, $M_* \lesssim 2$ M$_\odot$) is magnetospheric accretion (Hartmann 1998, and references therein). The stellar magnetic field threads the inner disk regions, and at some radius $R_{\rm mag}$, the ram pressure of accreting material is balanced by this magnetic pressure. Material is therefore no longer able to move inward through the disk midplane, but rather is funneled along magnetic field lines onto high-latitude regions of the star, where hot accretion shocks form. The alternative that may operate in more massive stars is boundary layer accretion, where material accretes through the disk midplane, forming a shock at the stellar equator (e.g., Lynden-Bell & Pringle 1974).

At some point, likely during the transition from Class II to Class III, accretion onto the central star ceases. This may occur when disks are completely depleted, due to a combination

of viscous accretion, stellar winds, and photo-evaporation (e.g., Hollenbach et al. 2000), or when accretion rates become low enough (due to disk depletion) that the inward pressure of infalling material is balanced by outward pressure from a stellar wind. At this point, the stellar wind may cause dispersal of whatever material remains in the disk, both by blowing out small grains by radiation pressure and causing larger grains to spiral inward because of Poynting-Robertson (PR) drag. The gas is also probably depleted at this stage, although the dispersal mechanism is not known. This marks the end of the protoplanetary disk phase.

1.1.4 Planet Formation

The prevalent theory of both terrestrial and giant planet formation is core accretion, also referred to as sequential accretion, where small dust grains collide and stick with each other, forming progressively larger bodies (e.g., Safronov 1969; Kusaka et al. 1970; Cameron 1973). Small ($\sim$ 1 μm) dust grains in the disk may grow to approximately meter-sized bodies through slow collisions that result in the formation of van-der-Waals or molecular bonds. Once bodies grow to larger than kilometer-sized, self-gravity becomes the dominant mechanism for holding bodies together after (typically binary) collisions. While growing bodies from meter to kilometer-sized by collisions remains an unsolved problem, very recent work suggests that effects such as gas drag, high porosity, or turbulent vortices may enable growth to kilometer-sized planetesimals (e.g., Wurm et al. 2001; Klahr & Bodenheimer 2004). The core accretion process requires $\gtrsim 10^7$ years to form Jupiter-mass planets (e.g., Bodenheimer & Pollack 1986; Pollack et al. 1996), longer than inferred lifetimes for protoplanetary disks (§1.2). However, various effects including orbital migration, gas drag, or turbulence, may lead to shorter formation timescales (e.g., Papaloizou & Terquem 1999; Rafikov 2004; Klahr & Bodenheimer 2004).

An alternative to core accretion, which has the potential to form massive planets over very short timescales, is gravitational instability (e.g., Cameron 1978; Boss 1997). In this theory, a very massive disk becomes highly gravitationally unstable and a fragment of the disk begins to collapse. The density of a typical fragment must be high enough to overcome both pressure and centrifugal forces: for typical assumptions for protoplanetary disks, these requirements lead to fragment masses on the order of a Jupiter mass for disk radii $\gtrsim$ 100 AU, and larger masses at smaller radii (e.g., Rafikov 2005). The timescale for this mass to collapse is on the order of the disk dynamical timescale, which may be hundreds or thousands of years (e.g., Boss 1997). Thus, gravitational instability has the potential to form gas giant planets in very little time. One potential problem is that unless mass is being added to the disk very rapidly, marginally-unstable disks may re-adjust themselves through non-axisymmetric instabilities to stable configurations before fragmentation can occur (Laughlin & Bodenheimer 1994). Moreover, if fragmentation does occur, these fragments must be able to cool quickly (faster than disk dynamical timescales), or else they will be mixed back into the disk before a self-gravitating body can form (e.g., Rafikov 2005).